Article

Cell Reports

Resolving Subcellular miRNA Trafficking and Turnover at Single-Molecule Resolution

Graphical Abstract

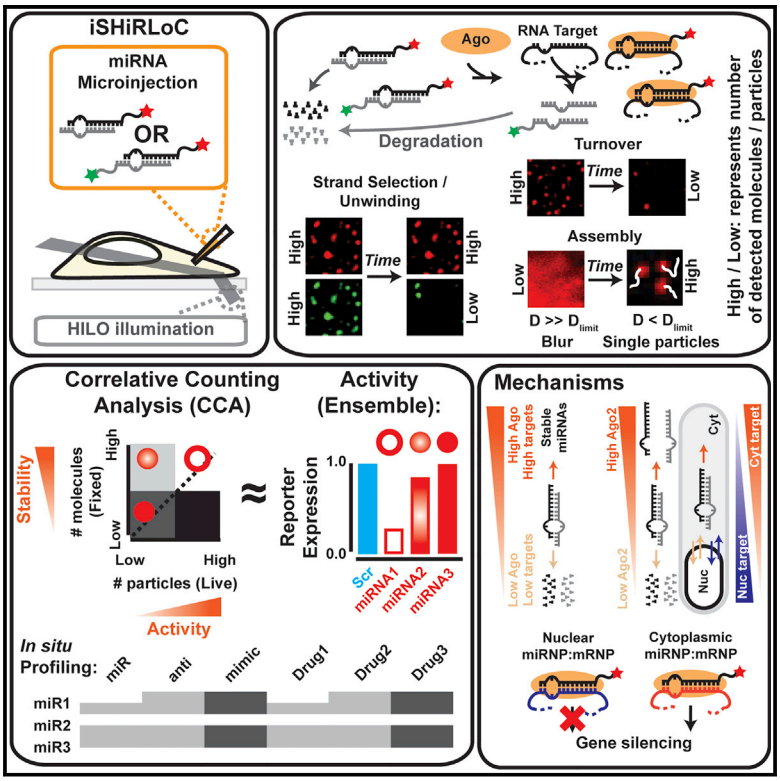

Highlights

- iSHiRLoC and CCA quantify miRNA unwinding, turnover, and activity inside cells
- miRNA stability and nuclear retention is dependent on Argonaute and targets
- miRNA unwinding, strand selection, and cytoplasmic retention are Ago2 dependent
- Nuclear miRNAs do not repress cognate targets

Authors

Sethuramasundaram Pitchiaya, Laurie A. Heinicke, Jun I. Park, Elizabeth L. Cameron, Nils G. Walter

Correspondence

nwalter@umich.edu

In Brief

Pitchiaya et al. describe tools to interrogate gene-regulatory microRNAs inside living cells at single-molecule resolution. They find that the RNA silencing machinery and RNA targets mediate gene silencing surveillance by modulating the abundance and subcellular location of microRNAs. These findings and tools promise to facilitate single-cell screening of microRNA activity.

Pitchiaya et al., 2017, Cell Reports *19*, 630–642
April 18, 2017
http://dx.doi.org/10.1016/j.celrep.2017.03.075

CellPress

OPEN ACCESS
CellPress

Cell Reports
Article

Resolving Subcellular miRNA Trafficking and Turnover at Single-Molecule Resolution

Sethuramasundaram Pitchiaya,[1,2] Laurie A. Heinicke,[1] Jun I. Park,[1,2] Elizabeth L. Cameron,[1] and Nils G. Walter[1,3,*]
[1]Single Molecule Analysis Group, Department of Chemistry, University of Michigan, Ann Arbor, MI 48109-1055, USA
[2]Present address: Michigan Center for Translational Pathology, University of Michigan Medical School, Ann Arbor, MI 48109-1055, USA
[3]Lead Contact
*Correspondence: nwalter@umich.edu
http://dx.doi.org/10.1016/j.celrep.2017.03.075

SUMMARY

Regulation of microRNA (miRNA) localization and stability is critical for their extensive cytoplasmic RNA silencing activity and emerging nuclear functions. Here, we have developed single-molecule fluorescence-based tools to assess the subcellular trafficking, integrity, and activity of miRNAs. We find that seed-matched RNA targets protect miRNAs against degradation and enhance their nuclear retention. While target-stabilized, functional, cytoplasmic miRNAs reside in high-molecular-weight complexes, nuclear miRNAs, as well as cytoplasmic miRNAs targeted by complementary anti-miRNAs, are sequestered stably within significantly lower-molecular-weight complexes and rendered repression incompetent. miRNA stability and activity depend on Argonaute protein abundance, whereas miRNA strand selection, unwinding, and nuclear retention depend on Argonaute identity. Taken together, our results show that miRNA degradation competes with Argonaute loading and target binding to control subcellular miRNA abundance for gene silencing surveillance. Probing single cells for miRNA activity, trafficking, and metabolism promises to facilitate screening for effective miRNA mimics and anti-miRNA drugs.

INTRODUCTION

MicroRNA(miRNA)-mediated gene silencing is a pervasive, evolutionarily conserved cellular pathway wherein endogenous small non-coding RNAs (ncRNAs) guide the RNA-induced silencing complex (RISC) to translationally repress and eventually degrade complementary sequence-matched mRNA targets (Pasquinelli, 2012). Biosynthesis of functional miRNAs follows a tightly regulated multi-step pathway, encompassing both the nuclear and cytoplasmic compartments of the cell (Ha and Kim, 2014; Lin and Gregory, 2015). Following the transcription of a miRNA gene, a primary miRNA transcript (pri-miRNA) is processed in the nucleus to generate a corresponding precursor-miRNA (pre-miRNA), which is then exported to the cytoplasm and further processed to yield mature, ~22-bp miRNA duplexes. One strand of the miRNA duplex (the guide strand [G]) is preferentially retained within the Argonaute (Ago) protein containing RISC, whereas the other strand (passenger [P], or "*") is released and possibly degraded. Activated microRNA-induced silencing complex (miRISC) then engages mRNAs by hybridizing the G strand with complementary seed sequences, leading to RNA silencing (Pasquinelli, 2012). Recent reports suggest that many RISC factors and mature miRNAs are also present in the nucleus, allowing for potentially widespread nuclear functions (Gagnon et al., 2014; Khudayberdiev et al., 2013; Liao et al., 2010; Weinmann et al., 2009; Zisoulis et al., 2012). Collectively, miRNAs regulate many developmental and physiological processes, and their dysregulation is known to lead to pathologies, including cancer (Lin and Gregory, 2015). The cellular abundance and subcellular localization of miRNAs is thus central to maintaining physiological homeostasis.

miRNA levels are regulated via both transcriptional and post-transcriptional mechanisms. Post-transcriptional regulation of miRNAs can occur via protein- or target RNA-mediated pathways. One protein-mediated pathway involves the regulation of the levels or activities of key role players in the miRNA biosynthesis pathway (Ha and Kim, 2014; Pasquinelli, 2012). Another pathway encompasses proteins, including the XRN1/2 5′-to-3′ (Chatterjee and Grosshans, 2009) and SDN 3′-to-5′ exonuclease complexes (Ramachandran and Chen, 2008), that directly mediate miRNA turnover (Kai and Pasquinelli, 2010). There is conflicting evidence, however, whether targets of miRNAs promote or rather inhibit turnover of mature miRNA. Brown and coworkers (Baccarini et al., 2011) reported that extensive complementarity between mRNA targets and miRNAs promotes miRNA degradation in human cells, suggesting that miRNA decay through 3′ uridylation is promoted by targets. Moreover, Zamore and coworkers have found evidence that targets promote 3′ adenylation and/or trimming of cognate miRNA 3′ ends to initiate degradation in *Drosophila* (Ameres et al., 2010). In contrast, mRNA targets have been shown to protect miRNAs in *C. elegans* (Chatterjee et al., 2011).

Recent reports suggest that sub-cellular localization is critical to miRNA function (Leung, 2015). In particular, the discoveries of mature miRNAs in the nucleus (Gagnon et al., 2014; Khudayberdiev et al., 2013; Liao et al., 2010) and of the ability of small RNAs to guide RNA target cleavage in the nucleus (Gagnon et al., 2014) were unexpected. Several groups have suggested

that engineered and exogenously added small RNAs and Ago proteins can mediate nuclear gene regulation in the forms of inhibition (Castanotto et al., 2005; Janowski et al., 2005, 2006; Kim et al., 2006; Morris et al., 2004; Napoli et al., 2009; Ting et al., 2005) or activation of transcription (Janowski et al., 2007; Li et al., 2006; Matsui et al., 2013) and of control over alternative splicing (Alló et al., 2009; Liu et al., 2012), but mechanisms mediating these processes largely remain unresolved. While import and export factors mediating the nucleo-cytoplasmic trafficking of mature miRNAs have been identified (Castanotto et al., 2009; Ohrt et al., 2006; Yi et al., 2003), factors that retain mammalian miRNAs in the nucleus and the kinetics associated with trafficking are largely unknown.

Consequently, there is an urgent need for approaches that can dissect miRNA localization, function, and turnover within the cellular environment. To this end, we previously reported the ability of intracellular single-molecule, high-resolution localization and counting (iSHiRLoC) to dissect two kinetically sequential miRNA assembly pathways in single HeLa cervical cancer cells (Pitchiaya et al., 2012, 2013). Here, we have extended iSHiRLoC to exploit single, microinjected, mature miRNA reporters for a comprehensive survey of the subcellular localization, maturation, turnover, and function of miRNAs. Our current technology interrogates RISC loading and subsequent steps of the miRNA-mediated RNA silencing pathway but is potentially extendable to investigate upstream pathway steps, simultaneously visualize small RNAs and RISC complexes, and probe target search mechanisms of RISC inside cells. Introducing a correlative counting analysis (CCA) of live- and fixed-cell images, we find that Ago proteins and seed-matched targets play a critical role in mediating nuclear retention and stabilization of mature miRNAs. In cells lacking Ago2, P strand discard is diminished and nuclear localization enhanced compared to cells either overexpressing Ago2 or lacking Ago1, suggesting additional non-redundant functions of nuclear Ago proteins. We further find that nuclear miRNAs are not as effective in silencing their cognate targets as their cytoplasmic counterparts. Our work reveals underappreciated roles of both cognate RNA targets and Ago2 in controlling subcellular miRNA abundance for surveillance of gene regulation.

RESULTS

iSHiRLoC Resolves miRNA Localization, Unwinding, and P Strand Removal

To dissect the RNA silencing pathway in mammalian cells, we expanded our previously established iSHiRLoC assay (Figure 1A). We used the highly conserved tumor suppressor miRNA let-7-a1 (henceforth l7/l7*, where l7 refers to the guide or G strand and l7* refers to the P strand, known to have ~1,200 mRNA targets in human cells per targetscan 7.1) (Roush and Slack, 2008) as a reporter and the flat, microscopically amenable human U2OS osteosarcoma cells as our model system. Based on prior reports that fluorophore labels on miRNAs do not affect the activity and binding kinetics of eukaryotic Ago in vitro (Chandradoss et al., 2015), we further confirmed that the conjugation of a fluorescent dye to the 3′ end of individual or both strands of a mature, double-stranded miRNA (ds-miRNA) does not affect their RNA silencing activity in U2OS cells (Figure S1). To avoid photobleaching of the miRNA-conjugated Cy3 or Cy5 dye during initial visualization of cells, microinjection samples were supplemented with a spectrally distinct, fluorescein- or Alexa-Fluor-405-labeled dextran. Hydrophilic dextrans are biologically inert and stable and cannot permeate through the cell membrane, so they are retained within cells (Ludtke et al., 2002). Moreover, high-molecular-weight (>70 kDa) dextrans are refractory to nucleo-cytoplasmic transport so that they remain within the intracellular compartment of microinjection (Kee et al., 2012). In addition to serving as a visual aid to identify cellular and nuclear boundaries, the co-injected dextrans were used henceforth as a loading control to normalize for the amount of material microinjected (Figures 1B, 1C, and S2).

Upon microinjection of just ~10,000 miRNA molecules, or less than 5% of the total cellular miRNA count, l7-Cy5/l7* assembled into spatially resolved, diffusing particles in living U2OS cells 2 hr after microinjection (Figure 1B), akin to our previous observation in HeLa cells (Pitchiaya et al., 2012, 2013). Using an optimized counting algorithm (Figure S2; Supplemental Experimental Procedures), we quantified the normalized subcellular abundance of diffusing particles and found that l7 predominantly remained in the cytoplasm, with a small yet significant fraction of 9% ± 3% found in the nucleus (Figure 1C). Consistent with our observations in HeLa cells (Pitchiaya et al., 2012, 2013), diffusion coefficients of cytosolic l7 in U2OS cells distributed within two Gaussian populations that resembled MS2-MCP-labeled mRNAs and GFP labeled P-bodies respectively (Figure 1D), as expected for a functional miRNA (Pitchiaya et al., 2012). To assess subcellular miRNA abundance more quantitatively, we performed stepwise photobleaching counting of similarly microinjected cells after fixation (Figure 1E). We found that >85% of all labeled particles contained only a single miRNA reporter molecule (Figure S2) and that 17% ± 4% of these molecules localized to the nucleus (Figures 1E and F). Considering that U2OS cells are only ~2.5–5 μm deep (Macdonald et al., 2013) and the depth of our highly inclined laminar optical sheet (HILO) illumination is ~3 μm (Liu et al., 2015), miRNAs present within the focal plane of illumination represent ~50% of all miRNAs in the cell (Figure S2).

In the cytosol, ds-miRNAs are unwound to retain the single-stranded G strand within RISC and to eject and possibly degrade the P strand. To further test for full functionality of our miRNA reporters, we performed two-color iSHiRLoC on fixed cells with the G and P strands of l7 miRNA labeled with spectrally distinct Cy5 and Cy3 dyes (l7-Cy5/l7*-Cy3), respectively (Figures 1A and 1G). Strikingly, we found that cells contained a large (>5-fold) excess of l7 over l7* in both cytoplasm and nucleus (Figure 1H,I), independent of dye identity (Figure S3), ruling out differential fluorescence detection sensitivity as a cause. These observations are consistent with the known asymmetric loading of l7 over l7* into RISC (Chatterjee et al., 2011), combined with loss of the ejected P strand due to RNA degradation and the expected expulsion of the resulting free dye from the cell (Homolya et al., 1993) or other forms of exocytic pathways. 2 hr after microinjection, less than 5% of G molecules still co-localized with P strand (Figure 1J), indicating that very few miRNA molecules are still double stranded and attesting to efficient loading of the guide. Taken together, our data establish iSHiRLoC as a quantitative

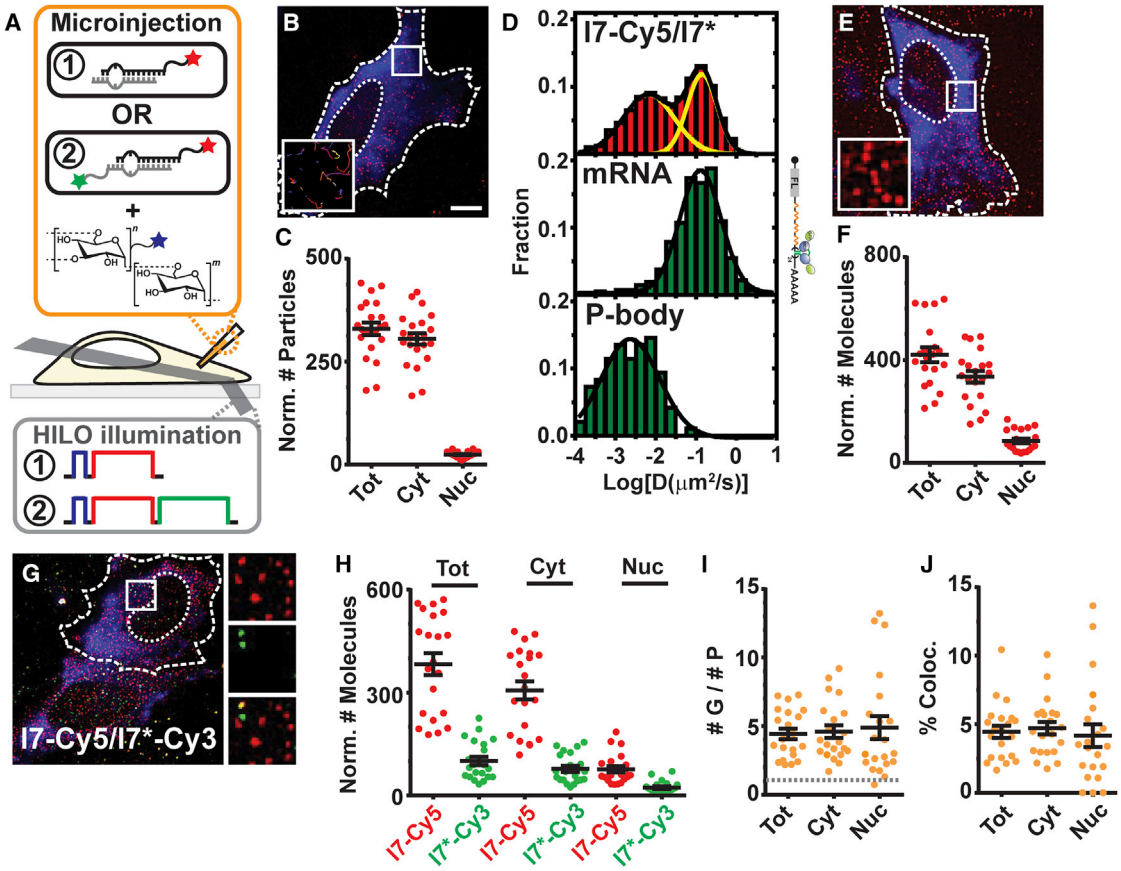

Figure 1. Outline of iSHiRLoC Data Acquisition and Analysis

(A) Schematic of iSHiRLoC assays. Singly (red only, "1") or doubly (red and green, "2"), 3′ end-labeled miRNAs and fluorophore-labeled dextran (blue) were co-microinjected into cells and imaged by HILO microscopy. Dextran (blue, 1 s), Cy5 (red, 30 s) and Cy3 (green, 30 s) were excited one after another, as represented in the schematic of excitation pulses.

(B) Representative image of a live U2OS cell containing stably assembled Cy5-labeled miRNA complexes as diffusing particles (red) and fluorescein-labeled, 500 kDa dextran (blue), 2 hr after microinjection into the cytosol. Dotted and dashed lines represent nuclear and cellular boundaries, respectively. Scale bar, 10 μm. Inset, 5.3 × 5.3 μm^2 represents zoomed-in tracks of particles within white box. Scale bar, 10 μm.

(C) Scatterplot depicting the total number of miRNA particles in the cell ("Tot") or within the cytoplasmic ("Cyt") or nuclear ("Nuc") compartments. Error bars represent SEM ($n \geq 3$, number of cells ≥ 18). Scale bars, labeling scheme and error bars are the same for other panels in this figure.

(D) Diffusion coefficient distribution of I7-Cy5/I7* miRNAs, MCP-GFP labeled firefly luciferase (FL) mRNA with the mH3UM 3′ UTR and GFP-Dcp1a punctate structures in U2OS cells.

(E) Representative image of a formaldehyde-fixed U2OS cell containing individual Cy5-labeled miRNA particles (red), a majority of which are individual molecules, and fluorescein-labeled, 500 kDa dextran (blue). Inset represents a zoomed-in view of particles within the white box.

(F) Scatterplot depicting the number of miRNA molecules.

(G) Representative image of formaldehyde-fixed U2OS cells containing individual particles I7-Cy5 and I7*-Cy3, and Alexa-Fluor-405-labeled, 500 kDa dextran (blue). Insets represent zoomed-in views of red (top), green (middle), and co-localized (bottom) particles within the white box.

(H) Scatterplot depicting the number of G and P strand molecules.

(I) Scatterplot representing the ratio of G to P strand. Gray line represents a 1:1 ratio of G:P.

(J) Scatterplot representing the percentage of co-localized molecules, as normalized to the more abundant G strand molecules.

single-molecule tool for detecting the subcellular localization, unwinding, and degradation of miRNAs in individual cells. Conversely, each cell in effect becomes an isolated reaction vessel for probing miRNA processing pathways.

Correlative Live- and Fixed-Cell Counting Probes miRNA Integrity and Activity

To verify that our microinjected ds-miRNAs functionally engage mRNA targets in the form of guide-strand loaded RISC, as opposed to merely hybridizing to complementary targets in the absence of a protein complex, we performed a series of iSHiRLoC assays with several RNA and DNA variants of I7/I7* miRNA. 2 hr after microinjection, I7-Cy5/I7* in live cells had again assembled into slowly diffusing RNPs (Figures 2A and 2B), which together with corresponding reporter gene assays (Figure 2C) indicated that I7 loaded RISC binds to and actively represses target mRNAs (Pitchiaya et al., 2012; Pitchiaya et al., 2013; Shankar et al., 2016). Strikingly, microinjecting an equivalent

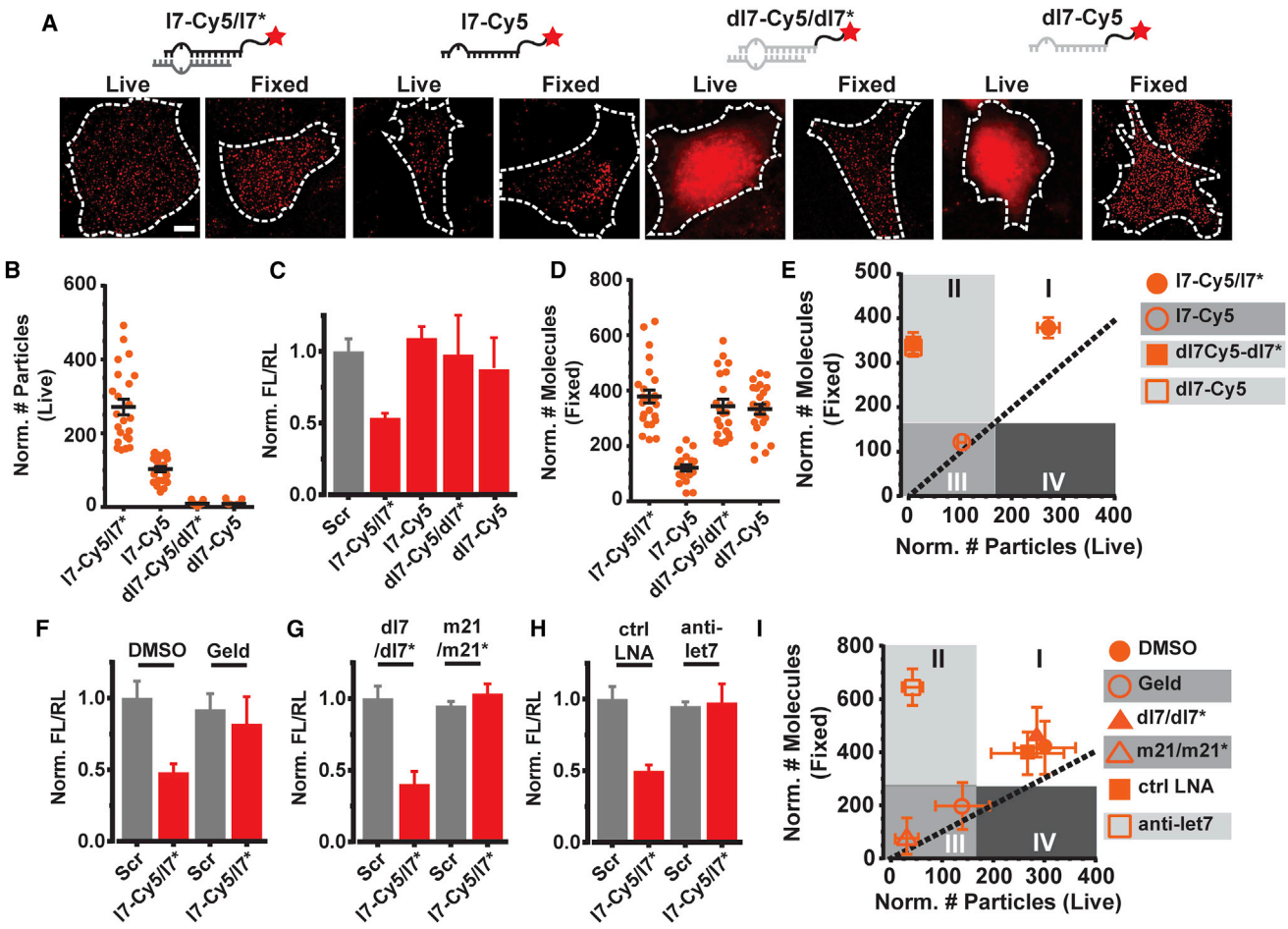

Figure 2. Validation of the CCA

(A) Representative images of live and fixed U2OS cells injected with various Cy5-labeled oligonucleotides (red) bearing the sequence of let-7 miRNA. Scale bar, 10 μm. Images were acquired 2 hr after microinjection.

(B) Scatterplot depicting the total number of particles for each "live" sample in (A). Error bars represent SEM ($n \geq 2$, number of cells ≥ 20).

(C) Luciferase reporter assays of U2OS cells transfected with the pmG-mH3U plasmid and the appropriate oligonucleotide. Error bars represent SEM (n = 3, with four technical replicates per trail).

(D) Scatterplot depicting the total number of molecules for each "fixed" sample in (A). Error bars represent SEM ($n \geq 2$, number of cells ≥ 20).

(E) Plot correlating the abundance of particles in live and fixed cells. Dotted line represents a perfect correlation. Each data point depicts the mean value, and error bars depict SEM. Shaded regions were arbitrarily chosen.

(F–H) Luciferase reporter assays of U2OS cells transfected with the pmG-mH3U plasmid and either a scrambled double-stranded oligonucleotide (Scr) or l7-Cy5/l7* under various treatment conditions. Error bars represent SEM (n = 3, with four technical replicates per trail). For inhibiting RISC loading (F), cells were treated with Geld and compared to control cells treated with DMSO. For competitive inhibition experiments (G), cells were treated with a 5-fold excess of unlabeled miR21 (m21/m21*) or an equivalent amount of dl7/dl7*. For blocking target binding (H), cells were treated with a 3-fold excess of anti-let7 anti-miR (LNA) or control anti-miR (ctrl LNA) bearing no complementarity to let7.

(I) Plot correlating the abundance of l7-Cy5/l7* particles in live and fixed cells, as plotted in (E).

quantity of single-stranded l7 (l7-Cy5) resulted in similarly diffusing complexes; however, the (normalized) number of such particles was significantly (~3-fold) less than for l7-Cy5/l7* (Figures 2A and 2B). This observation suggests that a majority of l7-Cy5 either resides in rapidly diffusing particles (with a diffusion constant >10 $\mu m^2/s$ and a molecular weight <0.5 MDa) that blur out at 100-ms time resolution (Liu et al., 2015; Pitchiaya et al., 2012) or is degraded and/or lost from the cell. To distinguish these possibilities, we performed iSHiRLoC's stepwise photobleaching counting in fixed cell (Pitchiaya et al., 2013) and found that the number of l7-Cy5 molecules was diminished by ~3-fold compared to l7-Cy5/l7*, very similar to our observations in live cells (Figures 2A–2D). These results suggest that single-stranded RNAs (ssRNAs) are actively degraded and the dye then expelled from the cell, similar to our observation for the unused P strand (Figure 1). Accordingly, the ssRNA does not downregulate a potential target in a gene reporter assay, unlike the corresponding dsRNA (Figure 2C). Further supporting our interpretation, guide-strand-labeled double-stranded DNA (dsDNA) or single-stranded DNA (ssDNA) versions of l7/l7*, expected to

be more stable intracellularly but incapable of RNA silencing, failed entirely to assemble into slowly diffusing RNPs (Figures 2A and 2B), even though their intracellular abundance in fixed cells remained high (Figures 2A and 2D), yet without regulatory potential (Figure 2C).

Since live-cell particle counting provided complementary information to our fixed-cell analysis, we correlated the two datasets within a comprehensive plot that we refer to here as CCA (Figure 2E). Plotting the live-cell imaging data on the x axis with the fixed-cell data on the y axis, we used the standard error of our data to empirically determine 35:65 and 30:70 splits of the x and y axes, respectively, to delineate the plot into four practically useful quadrants. Samples such as l7-Cy5/l7* that efficiently assemble into complexes diffusing like mRNPs in live cells and are stably retained as observed in fixed cells, will occupy the top right quadrant (Figure 2E, "I"). Samples prone to degradation, such as l7-Cy5, lead to low live- and fixed-cell counts and will occupy the bottom-left quadrant (Figure 2E, "III"). By contrast, stable samples that fail to assemble into slowly diffusing complexes but are retained in the cell, such as single-stranded or double-stranded let-7 DNA (dl7-Cy5 or dl7-Cy5/dl7*), will occupy the top-left quadrant of the plot (Figure 2E, "II"). Quadrant IV is populated when the particles identified in live cells exceed those identified in fixed cells, a scenario that typically manifests due to fixation induced dye photobleaching or loss from cell permeation. We find that quadrant IV is never populated in our assays. This correlative plot thus delineates the differences in intracellular behavior between species and further supports the notion that microinjected miRNAs act functionally through RNP assembly and not simple hybridization to mRNA targets.

To further test the robustness of our interpretation, we blocked two distinct steps of the RNA silencing pathway and performed iSHiRLoC-based correlative live/fixed-cell counting (Figures 2F–2I). First, we inhibited the loading of miRNA into RISC by treating cells with geldanamycin (Geld), an inhibitor of the Hsp90/Hsc70 chaperone, a known RISC loading factor (Iwasaki et al., 2010). Alternatively, we co-microinjected a 5-fold excess of unlabeled miR21 (m21/m21*) miRNA as a direct competitor for RISC loading. Finally, we co-microinjected an anti-miR complementary to l7 strand (anti-let7) to block target binding by the miRNA. All three strategies relieved miRNA mediated silencing in our luciferase gene reporter assay (Figures 2F–2H), in contrast to controls in which cells were treated with only DMSO (the geldanamycin solvent), with dark dl7/dl7*, or with a scrambled anti-miR (Figures 2F–2H), as expected. Concordantly, all three controls occupied quadrant I of the CCA plot, suggesting that the microinjected l7-Cy5/l7* stably assembled into functional RNPs (Figure 2I). In contrast, both strategies for blocking RISC loading shifted l7-Cy5 into quadrant III (Figure 2I), consistent with the miRNA no longer efficiently loading into RISC and consequently being degraded. Strikingly, anti-let7-treated cells occupied quadrant II of the plot (Figure 2I), indicative instead of intracellular stabilization of the miRNA within low molecular weight complexes of limited efficacy in engaging mRNAs. Our data thus suggest that 2 hr after microinjection, ~50%–80% of all observed miRNA molecules are stably retained inside cells as functional RNPs, while the rest are still undergoing RISC assembly or are involved in other cellular pathways. Our results also establish iSHiRLoC as a quantitative approach to dissecting miRNA integrity and activity.

Seed-Matched Targets Enhance Intracellular miRNA Stability

Based on the calibration of our microinjector (Pitchiaya et al., 2013), an intra-needle concentration of 1 μM should introduce ~10,000 molecules of miRNA per cell. 2 hr after microinjection, we typically observed only ~200–600 miRNA molecules per cell, suggesting that signal from a large fraction of molecules is lost due to degradation, expulsion from the cell, and/or other processes. To test for miRNA turnover and fluorophore expulsion from U2OS cells, we performed time courses of fixed- and live-cell counting of microinjected l7-Cy5/l7*-Cy3 and l7-Cy5/l7*, respectively. Observing fixed cells, loss of l7-Cy5 signal occurred in two distinct phases, fitted well with a double-exponential decay function (Figure 3A; Table S1). Signal loss was rapid during the first phase, i.e., within 1 hr after microinjection (t_1 ~20 min), with a second miRNA population observed to be lost 7-fold more slowly over the next several hours (t_2 ~8–24 hr) so that at 16 hr, no miRNAs were left (Figure 3A; Table S1). The half-life of l7-Cy5 measured using iSHiRLoC is similar to that of endogenous l7 in other cell lines (Rüegger and Großhans, 2012). Strikingly, at zero time, the fit intersects the y axis at ~9,700 molecules, consistent with the microinjection of ~10,000 molecules per cell (Table S1). Importantly, loss of l7* P strand was also biphasic and considerably more rapid throughout the time course (Figure 3A; Table S1), wherein a significant fraction of the molecules disappeared with a t_1 of ~7 min with the remaining molecules disappearing from the cells with a t_2 of 84 min. These data further corroborate our finding of asymmetric RISC loading of the G strand (Figure 1) and suggest that although a large fraction of the microinjected miRNA G strand is degraded, a significant fraction is stabilized over the P strand. Further supporting this view, in live cells, the appearance of slowly diffusing l7-Cy5 particles also occurred in two phases (Figure 3A), with the number of observable particles rapidly increasing within the first hour (t_1 ~6 min) and slowly disappearing from view (t_2 ~6 h) until no observable signal was detected 16 hr after microinjection. Taken together, these results suggest that a large fraction of l7/l7* molecules assemble as guide-strand-enriched miRISC (Figures 1, 2, and 3A), with a small-yet-significant fraction rapidly assembling into quite stable miRISC-mRNP complexes.

We next asked how the intracellular assembly and turnover of other miRNAs compares to l7/l7* by performing correlative live- and fixed-cell counting 2 hr after microinjection, when stable assembly of l7 was observed (Figure 3A). We found that a guide-strand-labeled let-7 seed mutant (ml7-Cy5/ml7*), which cannot repress targets with l7 binding sites (Figure S3C) and consequently has few intracellular targets, was rapidly turned over and unable to assemble into active miRISC-mRNP complexes, as indicated by a shift into quadrant III (Figure 3B). Similarly, the artificial cxcr4 miRNA (cx) and a negative control dsRNA (Scr), both of which have limited intracellular targets, were unstable and inefficiently assembled into diffusing complexes, also confining them to quadrant III (Figure 3B). By contrast,

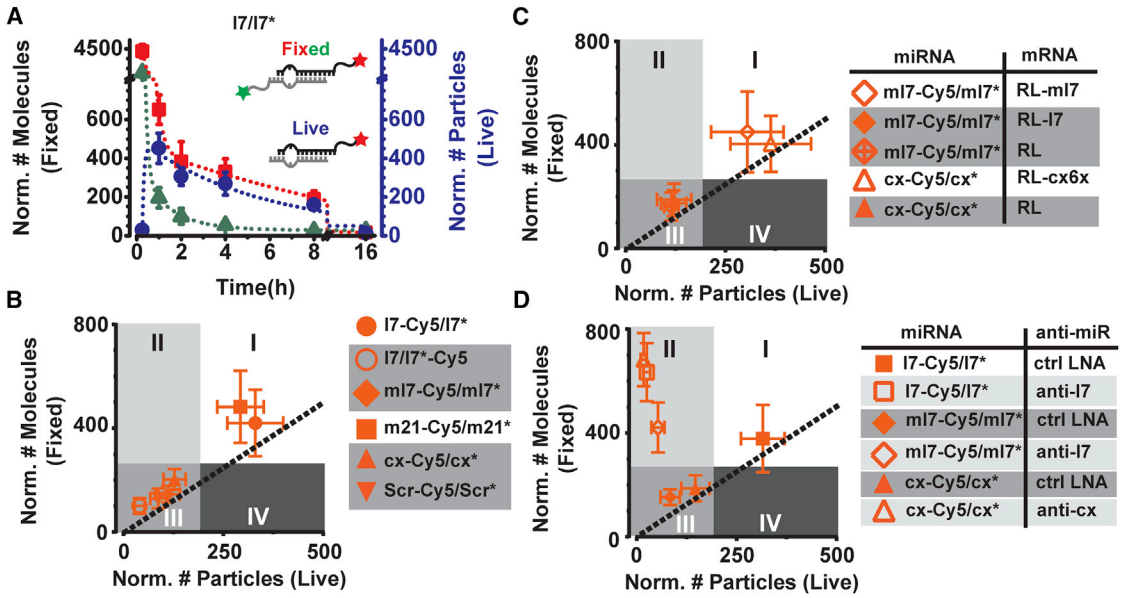

Figure 3. Seed-Matched Targets Protect miRNAs In Cellulo

(A) Time course analysis of microinjected let-7 abundance in live (blue) and fixed cells (green and red). Assays were done over a time course of 0.3–16 hr. The number of l7-Cy5 and l7*-Cy3 molecules in two-color iSHiRLoC assays are depicted in red (squares) and green (triangles), respectively, and their corresponding double-exponential fits are represented as appropriately colored dotted lines. iSHiRLoC live-cell assays using l7-Cy5/l7* miRNA were done on a complementary set of samples. Particle abundances are depicted in blue (circles), and the corresponding double-exponential fit is represented as a blue dotted line.

(B) CCA plot of various miRNAs 2 hr after microinjection.

(C) CCA plot of various miRNAs co-injected with target mRNAs 2 hr after microinjection. All miRNAs were labeled with Cy5 on the G and were co-injected with the appropriate target. RL-ml7 and RL-cx6x are seed-matched targets of ml7 and cx, respectively. RL-ml7 has two miRNA recognition elements (MREs) for ml7, whereas the RL-cx6x has six MREs for cx. RL-l7 bears a seed mismatch for ml7 at each of the MREs and is a target of l7, whereas RL mRNA does not have any 3′ UTR.

(D) CCA plot of various miRNAs co-injected with anti-miRs 2 hr after microinjection.

guide-strand-labeled miR-21 (m21-Cy5/m21*), which has ~300 distinct seed-matched targets in human cells (predicted by targetscan 7.1), stably assembled into miRISC-mRNP complexes and was found in quadrant I, next to l7 (Figure 3B). These data suggest that miRNA stability is correlated with the abundance of intracellular targets. To directly test whether seed-matched targets enhance miRNA stabilization and assembly into miRISC-mRNP complexes, we co-microinjected random, seed-mismatched, or seed-matched mRNA targets with the ml7-Cy5/ml7* or cx-Cy5/cx* miRNAs. As predicted, seed-matched targets mediated miRNA protection and miRISC-mRNP assembly, whereas all mismatches do not (Figure 3C).

Based on our previous observation that l7 is stabilized by anti-let7 in the form of small-molecular-weight complexes (Figure 2I), we reasoned that anti-miRs might act as "minimal" seed-matched targets. If so, seed-matched anti-miRs should generally mediate miRNA protection, just as the mRNA targets they mimic. We therefore co-microinjected various combinations of anti-miRs with either matched or mismatched miRNAs, confirming that only little anti-miR hybridized with the ds-miRNA in the injection needle (Figure S4A). As predicted, correlative live- and fixed-cell analysis showed that anti-cxcr4 miRNA robustly stabilized matched cx miRNA while not forming the slowly diffusing particles resembling miRISC-mRNP complexes, as evident from this combination appearing in quadrant II (Figure 3D). Indeed, an anti-miR generally shifts a matched or nearly matched miRNA into quadrant II (Figure 3D). Notably, anti-let-7 shifted the nearly matched mutant ml7-Cy5 into quadrant II but stabilized it less than the matched l7-Cy5, as evident from its lower fixed-cell count (Figure 3D). This observation is consistent with the only partial relief of ml7-mediated reporter gene repression by anti-let-7 (Figure S4B). We conclude that target-mediated miRNA protection (Chatterjee et al., 2011) can be observed in human cells, involves both mRNA and anti-miR targets, and competes with miRNA degradation to sustain intracellular gene silencing.

Mature miRNAs with mRNA Targets Localize to the Nucleus in Rapidly Diffusing Complexes

To understand the subcellular distribution and fate of mature miRNAs, we performed iSHiRLoC and CCA upon microinjecting l7-Cy5/l7* miRNA into the cytoplasm or nucleus of U2OS cells, as confirmed by imaging of the co-injected Alexa-Fluor-405-labeled high-molecular-weight dextran. Regardless of the compartment of injection, 2 hr after microinjection, a large majority of miRNAs had assembled into miRISC-mRNP complexes in the cytosol (quadrant I), with only a few remaining in the nucleus as low-molecular-weight complexes (quadrants II and III; Figures 4A and S5A). Notably, the retention of miRNAs in the nucleus was ~2-fold higher when first introduced there (Figures 4A and S5A). Consistent with previous reports for small interfering RNAs (siRNAs) (Ohrt et al., 2008), our data suggest that

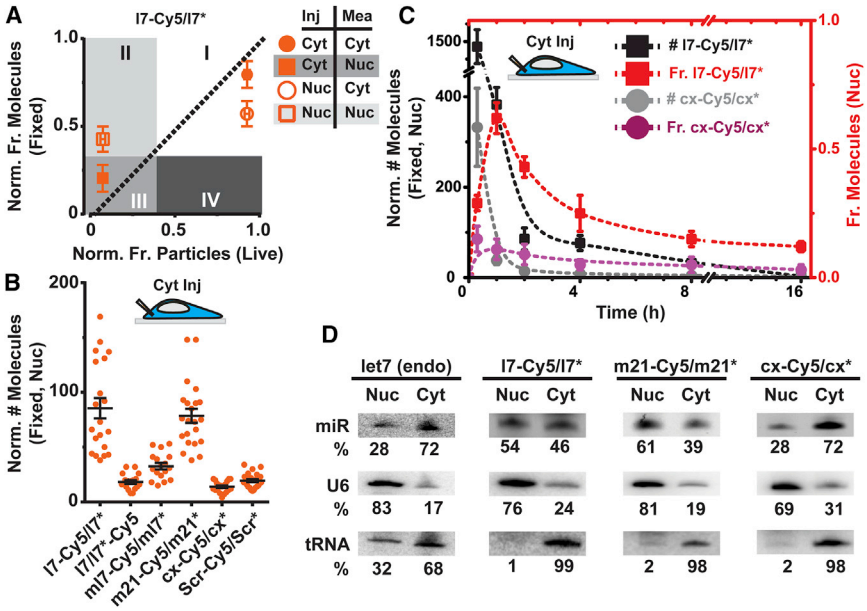

Figure 4. Mature miRNAs Localize in the Nucleus as Rapidly Diffusing Complexes, with the Extent of Localization Dependent on miRNA Sequence

(A) CCA plot of I7-Cy5/I7* when injected (Inj) in the cytosol (Cyt) or nucleus (Nuc) and measured (Mea) in the appropriate compartments ($n \geq 2$, ≥ 12 cells).

(B) Scatterplot representing the number of appropriate miRNA molecules in the nucleus ($n \geq 2$, ≥ 15 cells) when injected in the cytosol of U2OS cells.

(C) Time course analysis of nuclear I7-Cy5/I7* or cx-Cy5/cx* upon cytoplasmic injections. The molecular abundance in the nucleus (left y axis, # I7-Cy5/I7* and # cx-Cy5/cx*) and the nuclear fraction (right y axis, Fr. I7-Cy5/I7* and Fr. cx-Cy5/cx*) of each miRNA are represented ($n \geq 2$, ≥ 15 cells). t = 0 is an assumed data point, considering that all miRNAs are delivered directly into the cytosol during injection.

(D) Northern blot analysis of subcellular fractionated U2OS cells to detect endogenous (endo) or transfected miRNAs. Nuclear and cytoplasmic subcellular fractions are annotated as Nuc and Cyt. U6 small nuclear RNA (U6) and cytoplasmic tRNA-Lys serve as subcellular loading controls. Percentage of signal in each subcellular compartment has been corrected for leakage of U6 and tRNA-Lys and is mentioned below each blot (n = 2).

nuclear miRNAs assemble into low-molecular-weight complexes compositionally different from cytoplasmic high-molecular-weight miRISC-mRNP complexes.

To test the broader validity of our observations, we performed iSHiRLoC fixed-cell counting with a panel of miRNAs 2 hr after microinjection. While I7-Cy5/I7* and m21-Cy5/m21* localized in the nucleus of U2OS cells to similar extents, miRNAs without mRNA targets (mI7-Cy5/mI7*, cx-cy5/cx*, and Scr-Cy5/Scr*, as well as the P strand of let-7, i.e., I7/I7*-Cy5), generally displayed lower nuclear localization, independent of the compartment of microinjection (Figures 4B and S5B). Similar observations were made when I7-Cy5/I7* or cx-Cy5/cx* was instead microinjected into HeLa cells (Figure S5C). Analysis of I7 and cx miRNAs over a time course showed that significantly higher fractions of I7 were retained in the nucleus at any given time than cx, irrespective of the compartment of injection (Figures 4C and S5D; Table S2). We further found that an initial rapid influx of I7 miRNAs into the nucleus was followed by a slow efflux, whereas cx showed very little influx to begin with (Figures 4C and S5D; Table S1). These data suggest that nuclear localization appears to be specific to miRNAs with potential mRNA targets and that a G strand is preferentially retained in the nucleus over a P strand.

A previous report used oligofectamine-based transfection followed 24 hr later by subcellular fractionation and northern blotting to suggest that miR-29b accumulates in the nucleus of HeLa cells based on a hexanucleotide nuclear localization signal (Hwang et al., 2007). Using this experimental approach, U2OS cells transfected with fluorophore-labeled miRNAs indicated a more pronounced retention of I7 and m21 over cx in the nucleus (Figure 4D), consistent with our iSHiRLoC results. Notably, we found that transfection with lipofectamine generally retained miRNAs in the nucleus at 24 hr (Figure S5E), suggesting that this reagent is not ideal for localization studies. As a control, we also probed for endogenous I7 in U2OS cells, whose subcellular distribution closely matches that of our microinjected I7-Cy5/I7* but was different from transfected miRNAs, further supporting the notion that transfection, in contrast to microinjection, is not an ideal method of tracking miRNA localization. Next, we performed subcellular fractionation and northern blotting of HeLa cells transfected using oligofectamine and one of three different miR-29b variants to reproduce the previous work (Hwang et al., 2007). Surprisingly, we found that si-miR29a, a miRNA that does not to contain the hexanucleotide signal and was previously suggested to predominantly localize to the cytosol (Hwang et al., 2007), displayed similar nuclear abundance as si-miR29b and fluorophore-labeled miR-29b that both contain the signal (Figure S6A). Similarly, the extent of miR-29b nuclear localization after microinjection as measured by iSHiRLoC was similar to those of I7 and m21 in both U2OS and HeLa cells (Figures S6B and S6C). This suggests that miR-29b localizes significantly to the nucleus of human cells, but not more than other miRNAs with cellular mRNA targets that lack the previously described nuclear localization signal of miR-29b (Hwang et al., 2007). That is, nuclear miRNA localization appears to be primarily target driven.

Intracellular miRNA Unwinding and Nuclear Localization Are Dependent on Ago Identity

Small double-stranded oligonucleotides, such as miRNAs, siRNAs, and dsDNAs, used in our assays, are <40 kDa and therefore have the potential to passively shuttle across the nuclear membrane. To test whether target-dependent retention of miRNAs in the cell nucleus requires a saturable protein factor, we used our previous strategy (Figure 2) of blocking RISC loading with competing dsRNAs. We performed iSHiRLoC

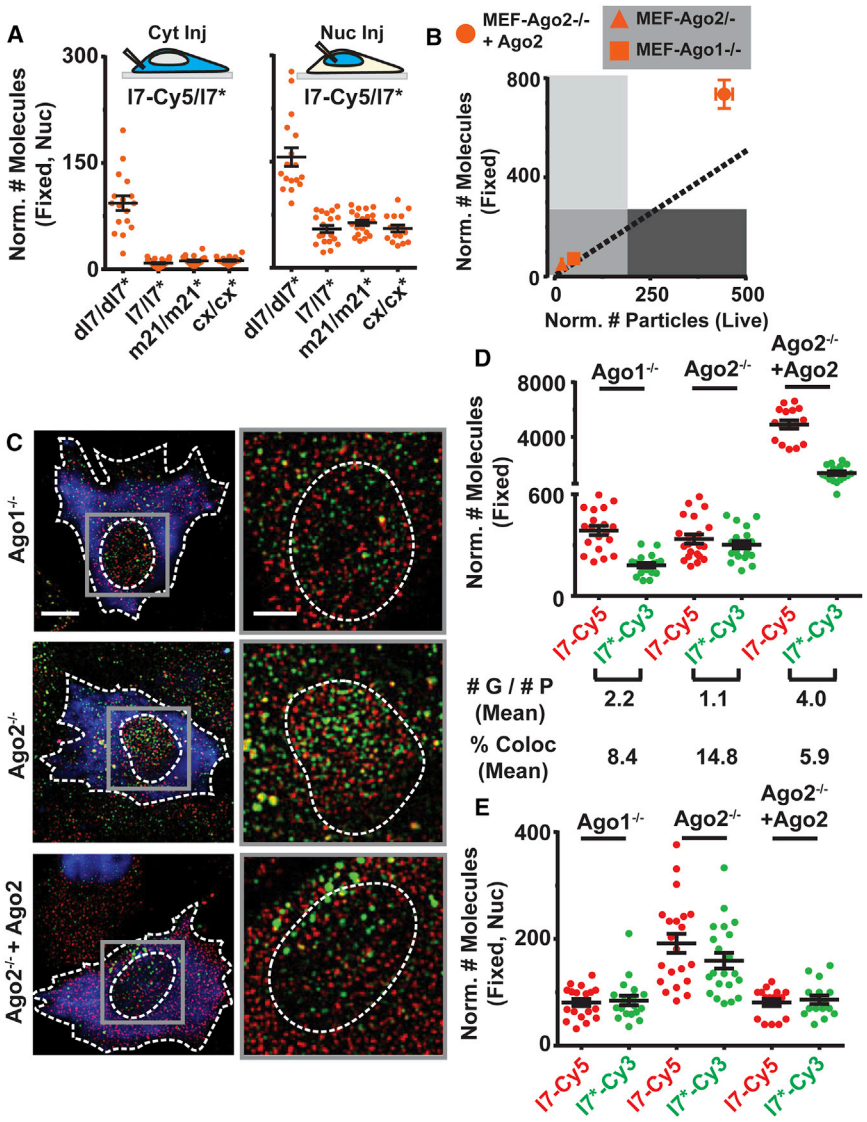

Figure 5. Ago Proteins Are Critical for Nuclear Localization and Unwinding of miRNAs

(A) Scatterplot representing the number of I7-Cy5/I7* molecules in the nucleus ($n \geq 2$, ≥ 15 cells) when co-injected with a let-7 dsDNA (dI7/dI7*) or unlabeled I7/I7*, m21/m21*, cx/cx* dsRNA. Samples were injected into the cytosol (left) or nucleus (right) of U2OS cells.

(B) CCA plot of I7-Cy5/I7* when injected in the cytosol of various MEF cells ($n \geq 2$, ≥ 10 cells).

(C) Representative, pseudocolored images of appropriate MEF cells injected in the cytoplasm with Alexa-Fluor-405-labeled 500 kDa dextran (blue) and I7-Cy5/I7*-Cy3 miRNA (Cy5, red; Cy3, green). Scale bar, 10 μm. Zoomed-in view of particles within gray box is depicted to the right of each image. Scale bar, 5 μm.

(D and E) Scatterplot depicting the number of G and P strand molecules throughout the appropriate MEF cell (D) or within the nucleus (E) is shown ($n \geq 2$, ≥ 15 cells) when injected in the cytosol of U2OS cells. The mean G:P ratio and % colocalization are mentioned below plot (D).

fixed-cell counting 2 hr after microinjecting mixtures of I7-Cy5/I7* with a 5-fold excess of unlabeled I7/I7*, m21/m21*, cx/cx*, or dI7/dI7* either into the cytoplasm or nucleus of U2OS cells. Nuclear localization of I7-Cy5 was diminished ~10-fold upon co-injection of competing dsRNAs into the cytosol compared to the control and ~3-fold when the RNA mixture was delivered directly into the nucleus (Figure 5A). These data suggest that a saturable protein factor and perhaps Ago loading are critical for nuclear localization of miRNAs. Next, we used two-color iSHiRLoC to test whether miRNAs are unwound when microinjected directly into the nucleus. To capture the rapidly degrading P strand (Figure 1), we performed these assays at the earliest possible time point just 20 min after microinjection. Strikingly, only 8%–15% of all I7 strands were still co-localized with I7*, although both strands were still found in the nucleus (Figures S7A–S7C). Additionally, I7 abundance was at least 2-fold higher than I7* levels (Figure S7C), very similar to our observations on miRNA unwinding upon cytoplasmic injection (Figures 1G–1J). Our data are consistent with the notion that miRNAs can be potentially unwound in the nucleus, in addition to the cytoplasm, and selectively retained in the nucleus.

Mammalian genomes encode four Ago isoforms, the relative expression of which depends on the cell type (Meister, 2013). The isoforms are thought to be functionally redundant in mediating canonical RNA silencing, but only Ago2 possesses endonucleolytic RNA cleavage ("slicer") activity. We therefore tested whether miRNA function and nuclear localization are dependent on Ago identity by employing a panel of three isogenic mouse embryonic fibroblast (MEF) cells that largely lack Ago1 (MEF-Ago1$^{-/-}$), lack Ago2 (MEF-Ago2$^{-/-}$), or overexpress Ago2 40-fold over the other two MEFs (MEF-Ago2$^{-/-}$+Ago2) (Broderick et al., 2011). Consequently, unlabeled mI7/mI7* repressed a cognate reporter with at least 10-fold less potency in MEF-Ago1$^{-/-}$ or MEF-Ago2$^{-/-}$ cells than in MEF-Ago2$^{-/-}$+Ago2 cells (Figure S7D; Table S3). 3′ fluorophore labeling of mI7 made these distinctions even more pronounced, as the miRNA was not functional in MEF-Ago1$^{-/-}$ or MEF-Ago2$^{-/-}$ cells even at high doses, whereas it robustly repressed its target in MEF-Ago2$^{-/-}$+Ago2 cells (Figure S7E). Consistent with these observations, CCA conducted 2 hr after microinjecting I7/I7* showed that the miRNA was highly destabilized in MEF-Ago1$^{-/-}$ and MEF-Ago2$^{-/-}$ cells (quadrant III; Figure 5B), whereas stable miRNA assembly into miRISC-mRNA complexes was observed in MEF-Ago2$^{-/-}$+Ago2 cells (quadrant I; Figure 5B). These data support the notions that Argonaute proteins can be a limiting silencing factor in cells (Broderick et al., 2011; Janas et al., 2012) and that, consequently, miRNA stability and

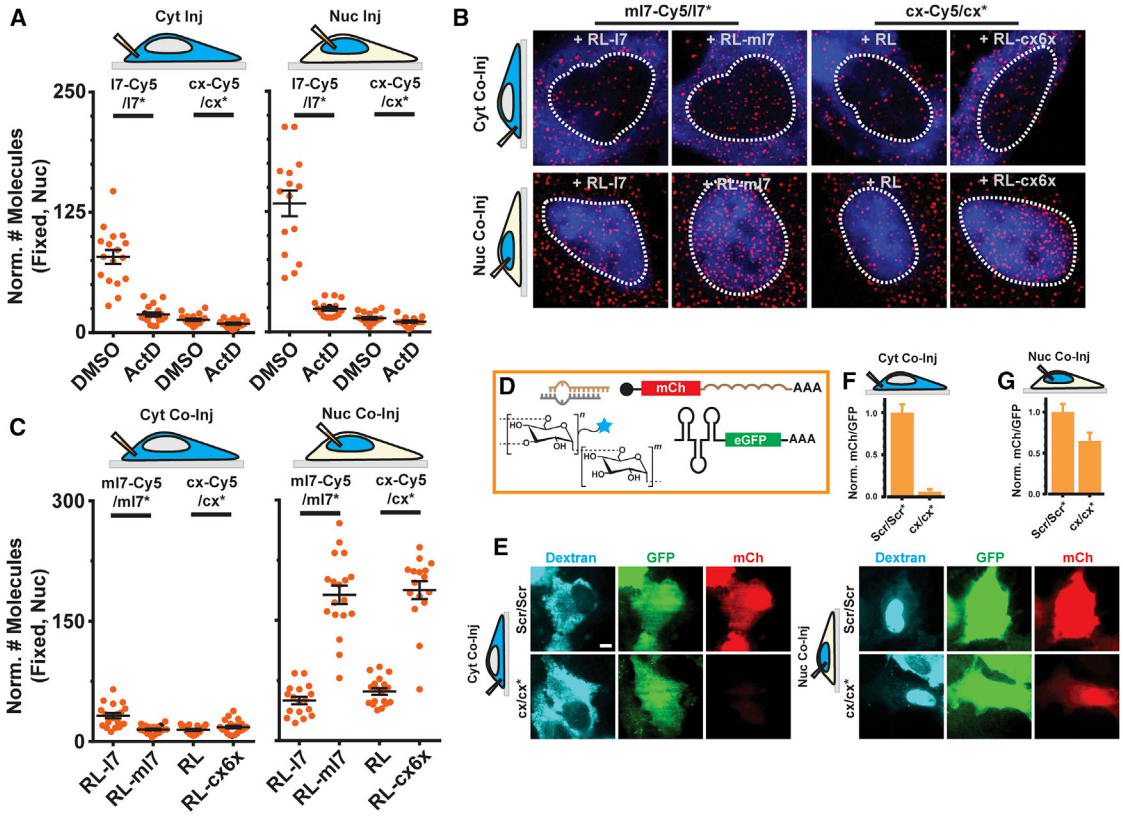

Figure 6. Seed-Matched Targets Mediate Nuclear Localization of miRNAs

(A) Scatterplot representing the number of l7-Cy5/l7* or cx-Cy5/cx* miRNA molecules in the nucleus of DMSO- or ActD-treated cells (n ≥ 2, ≥10 cells). Samples were injected into the cytosol (left) or nucleus (right) of U2OS cells and imaged 2 hr after microinjection.

(B) Representative, pseudocolored images of U2OS cells injected in the cytoplasm (top) or nucleus (bottom) with fluorescein isothiocyanate (FITC)-labeled 500 kDa dextran (blue), guide-strand-labeled miRNA (ml7-Cy5/ml7* or cx-Cy5/cx*, Cy5 – red), and unlabeled mRNA (RL-l7, RL-ml7, RL-cx6x or RL). Scale bar, 5 μm.

(C) Scatterplot depicting the quantifications of samples represented in (B) (n ≥ 2, ≥ 15 cells).

(D) Schematic of contents in microinjection needle.

(E) Representative images of dextran (blue), GFP (green), and mCherry (mCh, red) fluorescence in cells co-injected with a scrambled control RNA (Scr/Scr*) or cx/cx* in the cytosol (left panels) or nucleus (right panels) are shown. Scale bar, 10 μm.

(F and G) Quantifications of mCh fluorescence relative to GFP fluorescence for each sample are shown in (E). Error bars represent SEM.

repression activity are enhanced by increasing intracellular Ago levels, at the very least Ago2. To further test whether the lack of specific Ago proteins affects miRNA maturation and nuclear localization, we performed two-color iSHiRLoC fixed-cell counting on l7-Cy5/l7*-Cy3 at the earliest possible time point after microinjection (20 min). We observed, first, that the relative abundances of l7 and l7* were almost identical in MEF-Ago2$^{-/-}$ cells, as expected if both strands are degraded to similar extents; in contrast, there was asymmetric retention of l7 over l7* in both MEF-Ago1$^{-/-}$ and MEF-Ago2$^{-/-}$+Ago2 cells (Figures 5C and 5D). Consistent with our observation of limited stability upon depletion of either Ago1 or Ago2, however, the overall levels of l7 in MEF-Ago1$^{-/-}$ and MEF-Ago2$^{-/-}$ cells were similar and significantly (~10-fold) lower than those in MEF-Ago2$^{-/-}$+Ago2 cells (Figure 5D). Second, nuclear localization of both l7 and l7* was significantly (~2-fold) higher in MEF-Ago2$^{-/-}$ cells than in either MEF-Ago1$^{-/-}$ or MEF-Ago2$^{-/-}$+Ago2 cells (Figure 5E). Taken together, our data indicate that miRNA strand selection and unwinding are active only in cells that contain sufficient Ago2 and that a miRNA tends to be stabilized and retained particularly in the cytosol of such cells, whereas Ago1 (and perhaps Ago3 and Ago4) stabilizes miRNAs particularly in the nucleus without unwinding them. Ago2 thus has expanded functions in cytosolic gene silencing, beyond its endonucleolytic capabilities, whereas Ago1/3/4 appears to play a more dominant role in nuclear retention.

Seed-Matched RNA Targets Enhance Nuclear Retention of Mature miRNAs

To probe the role of RNA targets in nuclear retention of miRNAs directly, we performed iSHiRLoC fixed-cell counting of l7-Cy5/l7* and cx-Cy5/cx* miRNAs in U2OS cells treated for 4 hr with 5 μg/mL actinomycin D (ActD), a transcription inhibitor that drastically reduces levels of nascent transcripts (Bensaude, 2011; Figure S7F). As a result, the relative nuclear localization of l7-Cy5/l7*, 2 hr post-injection and incubation in ActD-containing media, was significantly reduced (~3- to 4-fold for cytoplasmic injections and 5- to 6-fold for nuclear injections), whereas that of cx-Cy5/cx* remained almost unaltered (Figure 6A). To verify

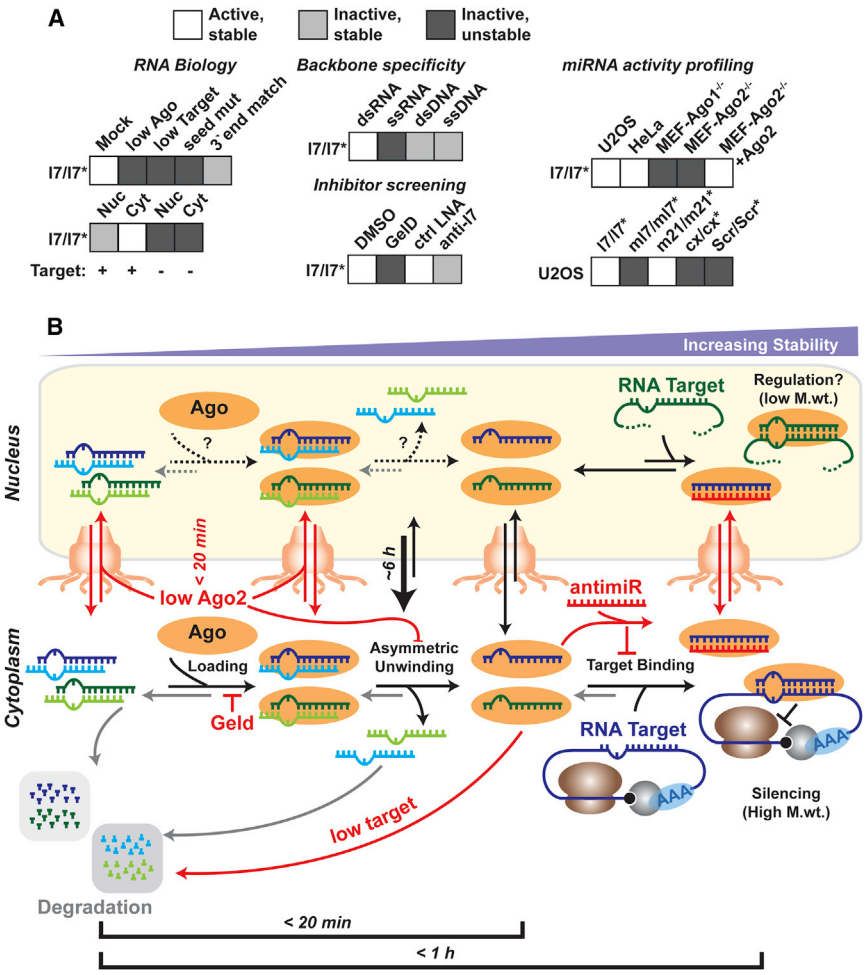

Figure 7. Summary of our Findings and Model Consistent with Our Data

(A) Inferences from CCA of miRNAs.

(B) A model depicting the time constants of assembly, turnover, and nucleo-cytoplasmic transport of miRNAs.

that targets are directly involved in nuclear retention of miRNAs, we co-microinjected either ml7-Cy5/ml7* or cx-Cy5/cx* miRNAs with random or seed-matched mRNA targets into the cytoplasm or nucleus of U2OS cells. We found that miRNAs are retained more strongly in their compartment of injection upon co-microinjection with cognate target (Figures 6B and 6C). Conversely, co-microinjection of mRNA with seed-matched miRNA allows for a particularly robust cytoplasmic mRNA expression (Figures 6D–6F), suggesting that a significant fraction of the mature mRNA is exported from the nucleus and its expression then not affected by the nucleus-retained miRNA. Cytoplasmic co-microinjection resulted in robust RNA silencing, confirming that microinjection does not affect canonical RNA silencing (Figures 6D–6F). Furthermore, we confirmed that a majority of the miRNA and mRNA molecules did not prematurely hybridize under our co-microinjection conditions in the needle (Figure S7G), suggesting that miRNA retention by nuclear RNA must involve active unwinding.

DISCUSSION

Small ncRNAs have been found to perform widespread structural, catalytic, and regulatory roles in the eukaryotic cell (Cech and Steitz, 2014), yet little is known about their spatiotemporal distribution and functionality within their native cellular environment. To bridge this gap, we here have refined our single-cell, single-molecule iSHiRLoC approach (Pitchiaya et al., 2012, 2013; Shankar et al., 2016) and applied it to mechanistically probe the miRNA-induced cytoplasmic RNA silencing pathway and its non-canonical nuclear counterpart. First, we validated our previous findings on the intracellular assembly of miRNAs (Pitchiaya et al., 2012), developed and validated a correlative live- and fixed-cell counting analysis to probe miRNA stability and function, and extended the applicability of iSHiRLoC to a wider range of cell types. Leveraging these advances, we further found that seed-matched RNA targets enhance miRNA stability and nuclear retention, with Ago1 playing a dominant role in recruiting miRNAs, without unwinding, into low-molecular-weight nuclear complexes. By contrast, Ago2 unwinds mature miRNAs and forms high-molecular-weight miRISC-mRNP complexes primarily in the cytoplasm.

Our human cell data unveil a fundamental competition between incorporation of mature miRNAs into the intracellular RNA silencing and degradation pathways (Figure 7), which is shifted toward silencing by the availability of Ago proteins and RNA targets. These observations are consistent with reports that Ago is typically a limiting factor in enabling miRNA activity (Broderick et al., 2011; Janas et al., 2012) and that the introduction of high levels of siRNAs in knockdown experiments can have side effects by competing with intracellular miRNAs (Khan et al., 2009) (Figures 2G and 5A). We additionally find that threshold target abundance is potentially crucial for miRNA protection (Figure 3). Of note, it is possible that the 3′ fluorophore on our miRNA probes suppresses 3′ tailing and trimming, which in turn decouples 3′ end remodeling from target-mediated effects, allowing us to corroborate target-mediated miRNA protection as a viable pathway for controlling miRNA levels, as previously described to occur during developmental processes (Chatterjee et al., 2011).

Strikingly, we find that MEF cells lacking Ago2 exhibit miRNA unwinding and localization profiles (Figure 5) distinct from those lacking Ago1. More specifically, miRNA unwinding was reduced in cells containing Ago1 but lacking Ago2, leading to both

strands of the miRNA localizing to the nucleus. This suggests that Ago2 mediates miRNA unwinding and promotes retention of miRNAs in the cytosol for canonical RNA silencing (Figure 7), expanding on the notion that mammalian Ago isoforms exhibit distinct miRNA binding/processing profiles and thus non-redundant functions (Meister, 2013).

Ago-bound small ncRNAs have been reported to perform important functions in the cellular nuclei of several lower organisms. For instance, small ncRNAs mediate RNA-induced transcriptional silencing (RITS) and epigenetic regulation in yeast, *C. elegans*, and plants, as well as transposon silencing in fruit flies (Castel and Martienssen, 2013). Moreover, the mammalian let-7 miRNA has been shown to regulate its own biogenesis, hypothetically via nuclear processing of its primary miRNA transcript (Zisoulis et al., 2012). The rapid uptake of our miRNA probes into the nucleus and their RNA target-dependent retention suggest that similar pathways may exist in mammals. Our data indicate that mammalian miRNAs play a role in nuclear-RNA-dependent processes such as transcription or splicing. In support of this hypothesis, miRNAs that were co-microinjected with cognate targets into the nucleus of mammalian cells were retained in the nucleus most strongly, even though the co-microinjected mature mRNAs were, as expected, efficiently exported into the cytoplasm, where they faced little RNA silencing from the largely nucleus-retained miRNAs (Figure 6).

Very few methods currently enable detection of single functional miRNAs in live or fixed cells. Tsourkas and coworkers have developed methods to count endogenous miRNAs in situ (Lu and Tsourkas, 2009), but only in formaldehyde-fixed cells that lose spatiotemporal features critical to living cells. Schwille and coworkers developed techniques based on microinjection and fluorescence correlation spectroscopy (FCS) to characterize diffusion properties of nuclear and cytoplasmic RISC (Ohrt et al., 2006, 2008) in live cells. However, the confocal illumination required by FCS only yield data from selected subsections of a mammalian cell at any given time, and deconvolving more than two molecular species of distinct mobility is challenging. Moreover, Schwille and coworkers typically investigated Ago2-bound miRNAs, with limited access to aspects of miRNA binding and turnover not requiring Ago2. We demonstrate here that our iSHiRLoC technique can account for all miRNA molecules introduced into a single cell at a defined zero time point and provides an unbiased, quantitative survey of intracellular pathways involving miRNAs at single-molecule resolution. In live-cell experiments, our typical 50–100 ms time resolution elegantly filters out "free" miRNAs (with a diffusion constant of 10–20 $\mu m^2/s$) and minimal RISC complexes (5–6 $\mu m^2/s$), both of which can be detected complementarily by FCS (Ohrt et al., 2008). Complementarily, fixed-cell iSHiRLoC experiments account for these complexes, as exemplified by the ability to detect stable yet non-functional miRNA-anti-miR complexes (Figure 3).

RNA therapeutics have exhibited remarkable promise in treating various pathologies (Kole et al., 2012), and a significant subset of these drugs target the miRNA pathway. For instance, anti-miR drugs that target miR-21 and miR-122 are currently in clinical trials for the treatment of Alport syndrome (Gomez et al., 2015) and pancreatic cancer (Sicard et al., 2013), respectively, as well as for hepatic pathologies (Haussecker and Kay, 2010). Moreover, miRNAs that mimic miR-34 activity (MRX34) have shown promise in targeting previously untreatable forms of cancer (Bouchie, 2013). iSHiRLoC uses individual cells as reaction vessels in ways that promise to facilitate screening for effective oligonucleotide-based drugs such as anti-miRs, especially in preclinical cell culture models, which has the potential to propel single-cell, single-molecule analysis into the realm of therapeutics.

EXPERIMENTAL PROCEDURES

Plasmids

Description of plasmids pmG-mH3U, pmG-mH3UM, pmG-cx6x, pEF6-mCh-cx6x, pEF6-mH, and pEF6-mHM can be found in Supplemental Experimental Procedures.

DNA and RNA Oligonucleotides

All DNA and RNA oligonucleotides used for iSHiRLoC experiments were obtained from IDT with a 5′ phosphate and, in the case of fluorophore-labeled oligonucleotides, a Cy3 or Cy5 dye at the 3′ end. G and P strands were heat-annealed in a 1:1.1 or 1:1 ratio, resulting in duplex miRNAs, and were frozen for further use. Negative control siRNA and siluc2 siRNA were purchased as ready-to-use duplex samples from Ambion and Dharmacon, respectively. Oligonucleotide sequences are listed in Tables S4 and S5.

mRNA Synthesis

In vitro transcriptions and mRNA purifications were performed as previously described (Pitchiaya et al., 2012).

Cell Culture

HeLa (CCL-2, ATCC) and U2OS (HTB-96, ATCC) cells were propagated as per the supplier's protocol. MEF cells, namely MEF-Ago1$^{-/-}$, MEF-Ago2$^{-/-}$, and MEF-Ago2$^{-/-}$ + Ago2, were obtained from Phil Zamore's lab and were propagated as described elsewhere (Broderick et al., 2011).

Luciferase Reporter Assays

100 μL of 10,000−20,000 cells were seeded per well of a 96-well plate. Transfection conditions and luminescence readouts are as described previously (Pitchiaya et al., 2012, 2013).

EMSA

Appropriate RNA samples were mixed with non-denaturing gel-loading buffer (10 mM Tris-HCl, 100 mM NaCl, 10 mM EDTA, 0.1% SDS, 0.02% NP40, and 10% glycerol) on ice, and 15 μL of each sample was loaded onto each well of a pre-cast 20% TBE gel (Life Technologies). Gels were run at 200 V for ~2.5 hr at 4°C.

Real-Time qPCR

U2OS cells were treated with DMSO or ActD (5 μg/μL) in regular medium for 0 hr or 4 hr in six-well plates and harvested, and total RNA was extracted and quantified by real-time qPCR. Primer sequences are listed in Table S6.

Biochemical Fractionation and Northern Blotting

Nucleo-cytoplasmic fractionation and northern blotting were performed as described previously (Gagnon et al., 2014; Hwang et al., 2007). Northern blotting probe sequences are listed in Table S5.

Microinjection

Cells grown on DeltaT dishes (Bioptechs) were microinjected as described elsewhere (Pitchiaya et al., 2012, 2013).

Microscopy and Image Analysis

Imaging and analysis was performed as described previously (Pitchiaya et al., 2012, 2013), with some minor modifications. Briefly, particle tracking analysis was performed using tracks that spanned at least four video frames. Stepwise

photobleaching analysis in fixed cells was done using custom written Lab-view codes and ImageJ.

Statistical Analysis

GraphPad Prism and Origin were used for statistical analysis and plotting. For pairwise comparisons, p values were calculated based on non-parametric unpaired t tests with Kolmogorov-Smirnov test. For comparisons involving more than two samples, one-way-ANOVA tests were used with Geisser-Greenhouse correction.

SUPPLEMENTAL INFORMATION

Supplemental Information includes Supplemental Experimental Procedures, seven figures, and six tables and can be found with this article online at http://dx.doi.org/10.1016/j.celrep.2017.03.075.

AUTHOR CONTRIBUTIONS

S.P. designed and performed all assays. L.A.H. performed the northern blotting analysis. E.J.C. assisted with microinjection experiments. J.I.P. assisted with reporter assays and EMSA. S.P. and N.G.W. conceived the study, and all authors wrote the manuscript.

ACKNOWLEDGMENTS

We thank D. Bartel, C. Mayr, C. Novina, R. Tsien, N. Kedersha, and R. Singer for generous gifts of plasmids containing the 3′ UTR of HMGA2, 3′ UTR of cxcr4, mCherry ORF, Dcp1a ORF, and the MS2 system of plasmids, respectively, P. Zamore for isogenic MEF cells, and A. Mapp and A. Chinnaiyan for access to their plate reader. This work was supported by National Institutes of Health (NIH) grants R01 GM081025 and GM062357 to N.G.W. and a fellowship from NIH Cellular Biotechnology training grant 4T32GM008353 to E.J.C.

Received: October 12, 2016
Revised: January 17, 2017
Accepted: March 28, 2017
Published: April 18, 2017

REFERENCES

Alló, M., Buggiano, V., Fededa, J.P., Petrillo, E., Schor, I., de la Mata, M., Agirre, E., Plass, M., Eyras, E., Elela, S.A., et al. (2009). Control of alternative splicing through siRNA-mediated transcriptional gene silencing. Nat. Struct. Mol. Biol. *16*, 717–724.

Ameres, S.L., Horwich, M.D., Hung, J.H., Xu, J., Ghildiyal, M., Weng, Z., and Zamore, P.D. (2010). Target RNA-directed trimming and tailing of small silencing RNAs. Science *328*, 1534–1539.

Baccarini, A., Chauhan, H., Gardner, T.J., Jayaprakash, A.D., Sachidanandam, R., and Brown, B.D. (2011). Kinetic analysis reveals the fate of a microRNA following target regulation in mammalian cells. Curr. Biol. *21*, 369–376.

Bensaude, O. (2011). Inhibiting eukaryotic transcription: Which compound to choose? How to evaluate its activity? Transcription *2*, 103–108.

Bouchie, A. (2013). First microRNA mimic enters clinic. Nat. Biotechnol. *31*, 577.

Broderick, J.A., Salomon, W.E., Ryder, S.P., Aronin, N., and Zamore, P.D. (2011). Argonaute protein identity and pairing geometry determine cooperativity in mammalian RNA silencing. RNA *17*, 1858–1869.

Castanotto, D., Tommasi, S., Li, M., Li, H., Yanow, S., Pfeifer, G.P., and Rossi, J.J. (2005). Short hairpin RNA-directed cytosine (CpG) methylation of the RASSF1A gene promoter in HeLa cells. Mol. Ther. *12*, 179–183.

Castanotto, D., Lingeman, R., Riggs, A.D., and Rossi, J.J. (2009). CRM1 mediates nuclear-cytoplasmic shuttling of mature microRNAs. Proc. Natl. Acad. Sci. USA *106*, 21655–21659.

Castel, S.E., and Martienssen, R.A. (2013). RNA interference in the nucleus: roles for small RNAs in transcription, epigenetics and beyond. Nat. Rev. Genet. *14*, 100–112.

Cech, T.R., and Steitz, J.A. (2014). The noncoding RNA revolution-trashing old rules to forge new ones. Cell *157*, 77–94.

Chandradoss, S.D., Schirle, N.T., Szczepaniak, M., MacRae, I.J., and Joo, C. (2015). A dynamic search process underlies MicroRNA targeting. Cell *162*, 96–107.

Chatterjee, S., and Grosshans, H. (2009). Active turnover modulates mature microRNA activity in Caenorhabditis elegans. Nature *461*, 546–549.

Chatterjee, S., Fasler, M., Büssing, I., and Grosshans, H. (2011). Target-mediated protection of endogenous microRNAs in C. elegans. Dev. Cell *20*, 388–396.

Gagnon, K.T., Li, L., Chu, Y., Janowski, B.A., and Corey, D.R. (2014). RNAi factors are present and active in human cell nuclei. Cell Rep. *6*, 211–221.

Gomez, I.G., MacKenna, D.A., Johnson, B.G., Kaimal, V., Roach, A.M., Ren, S., Nakagawa, N., Xin, C., Newitt, R., Pandya, S., et al. (2015). Anti-microRNA-21 oligonucleotides prevent Alport nephropathy progression by stimulating metabolic pathways. J. Clin. Invest. *125*, 141–156.

Ha, M., and Kim, V.N. (2014). Regulation of microRNA biogenesis. Nat. Rev. Mol. Cell Biol. *15*, 509–524.

Haussecker, D., and Kay, M.A. (2010). miR-122 continues to blaze the trail for microRNA therapeutics. Mol. Ther. *18*, 240–242.

Homolya, L., Holló, Z., Germann, U.A., Pastan, I., Gottesman, M.M., and Sarkadi, B. (1993). Fluorescent cellular indicators are extruded by the multidrug resistance protein. J. Biol. Chem. *268*, 21493–21496.

Hwang, H.W., Wentzel, E.A., and Mendell, J.T. (2007). A hexanucleotide element directs microRNA nuclear import. Science *315*, 97–100.

Iwasaki, S., Kobayashi, M., Yoda, M., Sakaguchi, Y., Katsuma, S., Suzuki, T., and Tomari, Y. (2010). Hsc70/Hsp90 chaperone machinery mediates ATP-dependent RISC loading of small RNA duplexes. Mol. Cell *39*, 292–299.

Janas, M.M., Wang, B., Harris, A.S., Aguiar, M., Shaffer, J.M., Subrahmanyam, Y.V., Behlke, M.A., Wucherpfennig, K.W., Gygi, S.P., Gagnon, E., and Novina, C.D. (2012). Alternative RISC assembly: binding and repression of microRNA-mRNA duplexes by human Ago proteins. RNA *18*, 2041–2055.

Janowski, B.A., Huffman, K.E., Schwartz, J.C., Ram, R., Hardy, D., Shames, D.S., Minna, J.D., and Corey, D.R. (2005). Inhibiting gene expression at transcription start sites in chromosomal DNA with antigene RNAs. Nat. Chem. Biol. *1*, 216–222.

Janowski, B.A., Huffman, K.E., Schwartz, J.C., Ram, R., Nordsell, R., Shames, D.S., Minna, J.D., and Corey, D.R. (2006). Involvement of AGO1 and AGO2 in mammalian transcriptional silencing. Nat. Struct. Mol. Biol. *13*, 787–792.

Janowski, B.A., Younger, S.T., Hardy, D.B., Ram, R., Huffman, K.E., and Corey, D.R. (2007). Activating gene expression in mammalian cells with promoter-targeted duplex RNAs. Nat. Chem. Biol. *3*, 166–173.

Kai, Z.S., and Pasquinelli, A.E. (2010). MicroRNA assassins: factors that regulate the disappearance of miRNAs. Nat. Struct. Mol. Biol. *17*, 5–10.

Kee, H.L., Dishinger, J.F., Blasius, T.L., Liu, C.J., Margolis, B., and Verhey, K.J. (2012). A size-exclusion permeability barrier and nucleoporins characterize a ciliary pore complex that regulates transport into cilia. Nat. Cell Biol. *14*, 431–437.

Khan, A.A., Betel, D., Miller, M.L., Sander, C., Leslie, C.S., and Marks, D.S. (2009). Transfection of small RNAs globally perturbs gene regulation by endogenous microRNAs. Nat. Biotechnol. *27*, 549–555.

Khudayberdiev, S.A., Zampa, F., Rajman, M., and Schratt, G. (2013). A comprehensive characterization of the nuclear microRNA repertoire of post-mitotic neurons. Front. Mol. Neurosci. *6*, 43.

Kim, D.H., Villeneuve, L.M., Morris, K.V., and Rossi, J.J. (2006). Argonaute-1 directs siRNA-mediated transcriptional gene silencing in human cells. Nat. Struct. Mol. Biol. *13*, 793–797.

Kole, R., Krainer, A.R., and Altman, S. (2012). RNA therapeutics: beyond RNA interference and antisense oligonucleotides. Nat. Rev. Drug Discov. *11*, 125–140.

Leung, A.K. (2015). The whereabouts of microRNA Actions: cytoplasm and beyond. Trends Cell Biol. *25*, 601–610.

Li, L.C., Okino, S.T., Zhao, H., Pookot, D., Place, R.F., Urakami, S., Enokida, H., and Dahiya, R. (2006). Small dsRNAs induce transcriptional activation in human cells. Proc. Natl. Acad. Sci. USA *103*, 17337–17342.

Liao, J.Y., Ma, L.M., Guo, Y.H., Zhang, Y.C., Zhou, H., Shao, P., Chen, Y.Q., and Qu, L.H. (2010). Deep sequencing of human nuclear and cytoplasmic small RNAs reveals an unexpectedly complex subcellular distribution of miRNAs and tRNA 3′ trailers. PLoS ONE *5*, e10563.

Lin, S., and Gregory, R.I. (2015). MicroRNA biogenesis pathways in cancer. Nat. Rev. Cancer *15*, 321–333.

Liu, J., Hu, J., and Corey, D.R. (2012). Expanding the action of duplex RNAs into the nucleus: redirecting alternative splicing. Nucleic Acids Res. *40*, 1240–1250.

Liu, Z., Lavis, L.D., and Betzig, E. (2015). Imaging live-cell dynamics and structure at the single-molecule level. Mol. Cell *58*, 644–659.

Lu, J., and Tsourkas, A. (2009). Imaging individual microRNAs in single mammalian cells in situ. Nucleic Acids Res. *37*, e100.

Ludtke, J.J., Sebestyen, M.G., and Wolff, J.A. (2002). The effect of cell division on the cellular dynamics of microinjected DNA and dextran. Mol. Ther. *5*, 579–588.

Macdonald, P., Johnson, J., Smith, E., Chen, Y., and Mueller, J.D. (2013). Brightness analysis. Methods Enzymol. *518*, 71–98.

Matsui, M., Chu, Y., Zhang, H., Gagnon, K.T., Shaikh, S., Kuchimanchi, S., Manoharan, M., Corey, D.R., and Janowski, B.A. (2013). Promoter RNA links transcriptional regulation of inflammatory pathway genes. Nucleic Acids Res. *41*, 10086–10109.

Meister, G. (2013). Argonaute proteins: functional insights and emerging roles. Nat. Rev. Genet. *14*, 447–459.

Morris, K.V., Chan, S.W., Jacobsen, S.E., and Looney, D.J. (2004). Small interfering RNA-induced transcriptional gene silencing in human cells. Science *305*, 1289–1292.

Napoli, S., Pastori, C., Magistri, M., Carbone, G.M., and Catapano, C.V. (2009). Promoter-specific transcriptional interference and c-myc gene silencing by siRNAs in human cells. EMBO J. *28*, 1708–1719.

Ohrt, T., Merkle, D., Birkenfeld, K., Echeverri, C.J., and Schwille, P. (2006). In situ fluorescence analysis demonstrates active siRNA exclusion from the nucleus by Exportin 5. Nucleic Acids Res. *34*, 1369–1380.

Ohrt, T., Mütze, J., Staroske, W., Weinmann, L., Höck, J., Crell, K., Meister, G., and Schwille, P. (2008). Fluorescence correlation spectroscopy and fluorescence cross-correlation spectroscopy reveal the cytoplasmic origination of loaded nuclear RISC in vivo in human cells. Nucleic Acids Res. *36*, 6439–6449.

Pasquinelli, A.E. (2012). MicroRNAs and their targets: recognition, regulation and an emerging reciprocal relationship. Nat. Rev. Genet. *13*, 271–282.

Pitchiaya, S., Androsavich, J.R., and Walter, N.G. (2012). Intracellular single molecule microscopy reveals two kinetically distinct pathways for microRNA assembly. EMBO Rep. *13*, 709–715.

Pitchiaya, S., Krishnan, V., Custer, T.C., and Walter, N.G. (2013). Dissecting non-coding RNA mechanisms in cellulo by single-molecule high-resolution localization and counting. Methods *63*, 188–199.

Ramachandran, V., and Chen, X. (2008). Degradation of microRNAs by a family of exoribonucleases in Arabidopsis. Science *321*, 1490–1492.

Roush, S., and Slack, F.J. (2008). The let-7 family of microRNAs. Trends Cell Biol. *18*, 505–516.

Rüegger, S., and Großhans, H. (2012). MicroRNA turnover: when, how, and why. Trends Biochem. Sci. *37*, 436–446.

Shankar, S., Pitchiaya, S., Malik, R., Kothari, V., Hosono, Y., Yocum, A.K., Gundlapalli, H., White, Y., Firestone, A., Cao, X., et al. (2016). KRAS engages AGO2 to enhance cellular transformation. Cell Rep. *14*, 1448–1461.

Sicard, F., Gayral, M., Lulka, H., Buscail, L., and Cordelier, P. (2013). Targeting miR-21 for the therapy of pancreatic cancer. Mol. Ther. *21*, 986–994.

Ting, A.H., Schuebel, K.E., Herman, J.G., and Baylin, S.B. (2005). Short double-stranded RNA induces transcriptional gene silencing in human cancer cells in the absence of DNA methylation. Nat. Genet. *37*, 906–910.

Weinmann, L., Höck, J., Ivacevic, T., Ohrt, T., Mütze, J., Schwille, P., Kremmer, E., Benes, V., Urlaub, H., and Meister, G. (2009). Importin 8 is a gene silencing factor that targets argonaute proteins to distinct mRNAs. Cell *136*, 496–507.

Yi, R., Qin, Y., Macara, I.G., and Cullen, B.R. (2003). Exportin-5 mediates the nuclear export of pre-microRNAs and short hairpin RNAs. Genes Dev. *17*, 3011–3016.

Zisoulis, D.G., Kai, Z.S., Chang, R.K., and Pasquinelli, A.E. (2012). Autoregulation of microRNA biogenesis by let-7 and Argonaute. Nature *486*, 541–544.